

Electrical-transport characteristics of as-grown and oxygen-reduced $\text{La}_{0.7}\text{Ce}_{0.3}\text{MnO}_3$ films: calculation of hopping energies, Mn valences, and carrier localization lengths

A Thiessen¹, E Beyreuther¹, R Werner², R Kleiner², D Koelle² and L M Eng¹

¹Institut für Angewandte Photophysik, Technische Universität Dresden, D-01062 Dresden, Germany

²Physikalisches Institut and Center for Collective Quantum Phenomena in LISA⁺, Universität Tübingen, Auf der Morgenstelle 14, D-72076 Tübingen, Germany

E-mail: andreas.thiessen@iapp.de, elke.beyreuther@iapp.de

Abstract. Presently, cerium-doped LaMnO_3 is vividly discussed as an electron-doped counterpart prototype to the well-established hole-doped mixed-valence manganites. Here, $\text{La}_{0.7}\text{Ce}_{0.3}\text{MnO}_3$ thin films of different thicknesses, degrees of CeO_2 phase segregation, and oxygen deficiency, grown on SrTiO_3 single crystal substrates, are compared with respect to their resistance-*vs.*-temperature (*R vs. T*) behavior from 300 K down to 90 K. While the variation of the film thickness (and thus the degree of epitaxial strain) in the range between 10 nm and 100 nm has only a weak impact on the electrical transport, the degree of oxygen deficiency as well as the existence of CeO_2 clusters can completely change the type of hopping mechanism. This is shown by fitting the respective *R-T* curves with three different transport models (adiabatic polaron hopping, Mott variable-range hopping, Efros-Shklovskii variable-range hopping), which are commonly used for the mixed-valence manganites. Several characteristic transport parameters, such as the hopping energies, the carrier localization lengths, as well as the Mn valences are derived from the fitting procedures.

PACS numbers: 71.30.h, 75.47.Lx, 73.61.Ng

1. Introduction

Doped rare-earth manganites (also referred to as mixed-valence manganites [1] or colossal magnetoresistive (CMR) manganites [2]) have been in the focus of intense scientific interest for several decades due to their peculiar magnetic/electrical phase diagrams, their magnetoresistance, and the subtle interplay between different (lattice, charge, spin, orbital) degrees of freedom. In the early years, fundamental issues such as the explanation of the relation between electrical transport and magnetic order in bulk crystals were in the focus [3, 4, 5]. Later, especially with the decisive progress in thin film preparation [6], a number of further intriguing issues were under debate, e.g., questions related to the functionalization of heterostructures and interfaces, electronic phase separation [7], or the response to light excitation [8].

Concerning the research field of functional heterostructures, such as all-manganite junctions [9, 10, 11], the possibilities of preparing electron-doped counterparts to the well-known hole-doped (lanthanum) manganites have been investigated for almost two decades. In the well-established case of the hole-doped La manganites, *divalent* cations such as Ca^{2+} or Sr^{2+} replace part of the La^{3+} ions, and concurrently force an equivalent number of Mn ions into the 4+ state to preserve charge neutrality. The resulting mixed 3+/4+ Mn valence goes along with the double exchange mechanism connected to a number of manganite-typical properties such as a metal-insulator transition associated with a ferromagnetic-paramagnetic phase transition and (at least in thin films) the colossal magnetoresistance effect. On the other hand, substituting part of the La^{3+} ions in the LaMnO_3 host lattice by *tetravalent* cations such as Ce^{4+} , Te^{4+} , or Sb^{4+} leads to a nominal electron-doping, connected with a mixed $\text{Mn}^{2+}/\text{Mn}^{3+}$ valence, the latter being supposed to be equivalent to the mixed 3+/4+ case with respect to the double-exchange mechanism [12]. Here, the cerium-doped LaMnO_3 , typically in the form of epitaxial $\text{La}_{0.7}\text{Ce}_{0.3}\text{MnO}_3$ (LCeMO) thin films [13], plays the role of a model compound for studying electron-doped lanthanum manganites. However, as shown by a growing body of experimental data, as-prepared LCeMO films tend to oxygen excess and thus an effective hole-doping (see e.g. [14] and refs. therein), while oxygen reduction by post-deposition annealing can indeed produce Mn valences below 3+, typically followed by the loss of the manganite-typical metal-insulator transition, producing films which are insulating across the whole temperature range [8]. A recent study by Middey et al. [15] demonstrated that LCeMO thin films grown layer-by-layer with pulsed laser interval deposition showed already in the as-prepared state electron doping but remained insulating in the whole temperature range, too. Attributed to the large variety of chemical compositions of manganite compounds (of which a number still waits for an in-depth analysis of its physical parameters) comprehensive electrical-transport data of this electron-doped state in $\text{La}_{0.7}\text{Ce}_{0.3}\text{MnO}_3$ films has rarely been reported to date, which is exactly the starting point of the work presented here.

2. Experimental

Pulsed laser deposition (PLD) was employed to grow three different $\text{La}_{0.7}\text{Ce}_{0.3}\text{MnO}_3$ films on SrTiO_3 (100) single crystal substrates. The exact growth conditions and the results of the structural analysis can be found in reference [16], the most important parameters (sample label / film thickness / oxygen partial pressure during PLD / result of the x-ray diffraction analysis) are listed here:

- B / 30 nm / 0.25 mbar / single-phase,[‡]
- C / 100 nm / 0.25 mbar / single-phase,
- D / 100 nm / 0.03 mbar / CeO_2 clusters.

As in our previous works on LCeMO [14, 17], which focused on the investigation of the Mn valence by photo-emission spectroscopy, the samples were investigated in different states of oxygen content:

- the *as-prepared* state,
- a *slightly reduced* state by heating in ultrahigh vacuum (10^{-9} mbar) at 480°C for 1 h, and
- a *highly reduced* state by heating in ultrahigh vacuum (10^{-9} mbar) at 700°C for 2 h.

To link the present measurements to our previous investigations, see refs. [8, 14, 17], the transport measurements of the as-prepared samples were compared to the results of a 10-nm LCeMO thin film, referred to as *sample A*, which was already subject of these former studies.

The resistance R of the LCeMO films was measured in the dark as a function of the temperature T in a nitrogen-cooled cryostat (Optistat DN by Oxford Instruments). Electrical contacts with a 3-mm distance were made by conductive silver paste on the LCeMO surfaces. To prevent leakage currents but guarantee good thermal contact the samples were mounted by conductive silver paste on a sapphire plate, while the temperature was measured by a Pt-100 resistor mounted on the same sapphire plate directly besides the sample. Since in all cases the LCeMO resistance was orders of magnitude higher than the wiring resistance, the measurements were performed in two-point geometry using a Keithley 6517B electrometer with a constant measuring voltage of 1 V, unless stated otherwise.

3. Theoretical background

For convenience, and also since the relevant information appears to be quite scattered throughout the literature, we summarize the most important knowledge concerning charge transport models for the insulating paramagnetic phase of mixed-valence manganites.

In the insulating phase the charge carriers are – at least partially – localized, and thus are not subject to a coherent band transport as it is the case in conventional semiconductors, but *move diffusively by thermally activated hopping between the Mn ions*. Thus the temperature dependence of the conductivity $\sigma(T)$ is inherently related to the hopping frequency $p(T)$ via:

$$\sigma(T) = \frac{x(x-1)}{c^3} \frac{e^2 r^2}{k_B T} p(T) \quad , \quad (1)$$

with c being the lattice constant, x the Mn^{4+} or Mn^{2+} concentration for hole or electron doped compounds, respectively, e the elementary charge, k_B the Boltzmann constant, and r the distance between two states assumed to be equivalent within $k_B T$ [18]. For the temperature dependence of the hopping probability (hopping frequency) $p(T)$ several variable-range hopping (VRH) [19, 20, 21] models, adiabatic polaron hopping (APH) [18, 22, 23] models, or combinations of both [24, 25] were reported in the literature. Briefly, the concepts behind APH and VRH are explained in the following:

3.1. Adiabatic polaron hopping

Due to strong electron-phonon coupling, the carriers distort the crystal lattice in their surroundings. Whenever the characteristic energy of this interaction is low compared to the conduction-band width, the carriers can further contribute to the coherent band transport, but the induced lattice polarization will follow the carriers, the latter thus exhibiting a large effective mass. Both, the electron and the lattice polarization form a quasiparticle, the so-called *large polaron* [26]. For mixed-valence manganites, however, the electron-phonon coupling is strong compared to the bandwidth. Thus, the carriers become trapped in potential wells built by the lattice distortions, hence revealing *small polarons*. In this case, thermally activated hopping may occur. Since lattice movements are slow compared to the hopping velocities, the term *adiabatic* is used for this process.

[‡] Though appearing single-phasic in the XRD analysis, a transmission electron microscopy study showed the existence of nanoscopic CeO_2 clusters for samples equivalent to B and C [16].

Within the framework of this APH model, which has been described by Edwards [23] in detail, the following relation is derived for σ :

$$\sigma(T) \propto T^{-1} \exp\left(-\frac{E_h}{k_B T}\right), \quad (2)$$

with E_h being the hopping energy, connected to the polaron binding energy E_p via $E_h = E_p/2$ for oxides in general [27] and via $E_h = E_p/4$ for manganites [23].

3.2. Variable-range hopping

If the Fermi level is located within a part of the conduction band which is localized by disorder, charge transport is possible either by thermal excitation into an empty and non-localized part of the band or by thermally activated hopping between localized states. The first case is relevant at high temperatures and results in the common thermally-activated band transport, while the latter case leads to the concept of the variable-range hopping as is relevant for the manganites. The term *variable-range* is derived from the fact that in this scenario the hopping distances (either between next neighbours or larger) can be, from energetic considerations, different, depending on the temperature.

The VRH theory, as described by Mott in ref. [28], results in the following temperature-dependent conductivity:

$$\sigma(T) \propto T^{-1/4} \exp\left[-\left(\frac{T_M}{T}\right)^{1/4}\right], \quad (3)$$

with the Mott temperature T_M calculated as:

$$T_M = \frac{\alpha_M}{k_B N(E_F) a^3}. \quad (4)$$

Here, α_M is a variable number between 10 and 27 (depending on the exact derivation [29]), a the localization length of the charge carrier, and $N(E_F)$ the density of states at the Fermi level. T_M is typically extracted as a fit parameter from the experimental conductivity-vs.-temperature data. From T_M the corresponding hopping energy E_M and the hopping distance r can be obtained according to:

$$E_M = k_B T \left(\frac{T_M}{T}\right)^{1/4}; \quad r = a \left(\frac{T_M}{T}\right)^{1/4}. \quad (5)$$

The Mott-VRH model was modified by Efros and Shklovskii by including the influence of electron correlation on the density of states which leads to the formation of a parabolic gap in the density of states at the Fermi energy [30], the so called Coulomb gap Δ_C . The temperature dependence of σ then reads as:

$$\sigma(T) \propto T^{-1/2} \exp\left[-\left(\frac{T_{ES}}{T}\right)^{1/2}\right], \quad (6)$$

with T_{ES} being the Efros-Shklovskii temperature:

$$T_{ES} = \frac{2.8e^2}{k_B \epsilon_0 \epsilon_r a}. \quad (7)$$

Unlike T_M , T_{ES} is independent of the density of states but depends on the dielectric constant ϵ_r . In the Efros-Shklovskii (ES) VRH model, the hopping energy and distance are calculated as follows:

$$E_{ES} = k_B T \left(\frac{T_{ES}}{T}\right)^{1/2}; \quad r = a \left(\frac{T_{ES}}{T}\right)^{1/2}. \quad (8)$$

The ES-VRH model becomes valid as soon as the hopping energy E_M is smaller than the Coulomb gap Δ_C , which is defined as:

$$\Delta_C = \frac{e^3 N(E_F)^{1/2}}{(\epsilon_0 \epsilon_r)^{3/2}}. \quad (9)$$

For the interpretation of the hopping transport within a very large temperature range in CMR manganites, Laiho et al. [25, 31] have extended the ES-VRH model by taking into account some peculiarities like the high temperatures at which VRH is observed in CMR manganites. Additionally, they took the influence of a temperature dependent rigid polaronic pseudo gap in the density of states [23, 32], Δ_{pg} , into account and deduced the following temperature dependence of the conductivity:

$$\sigma(T) \propto T^{-9/2} \exp\left[-\left(\frac{T_0}{T}\right)^{1/2}\right], \quad (10)$$

with T_0 being calculated as:

$$T_0 = \left[\frac{\Delta_{pg}}{2k_B T^{1/2}} + \left(\frac{\Delta_{pg}^2}{4k_B^2 T} + T_{ES} \right)^{1/2} \right]^2. \quad (11)$$

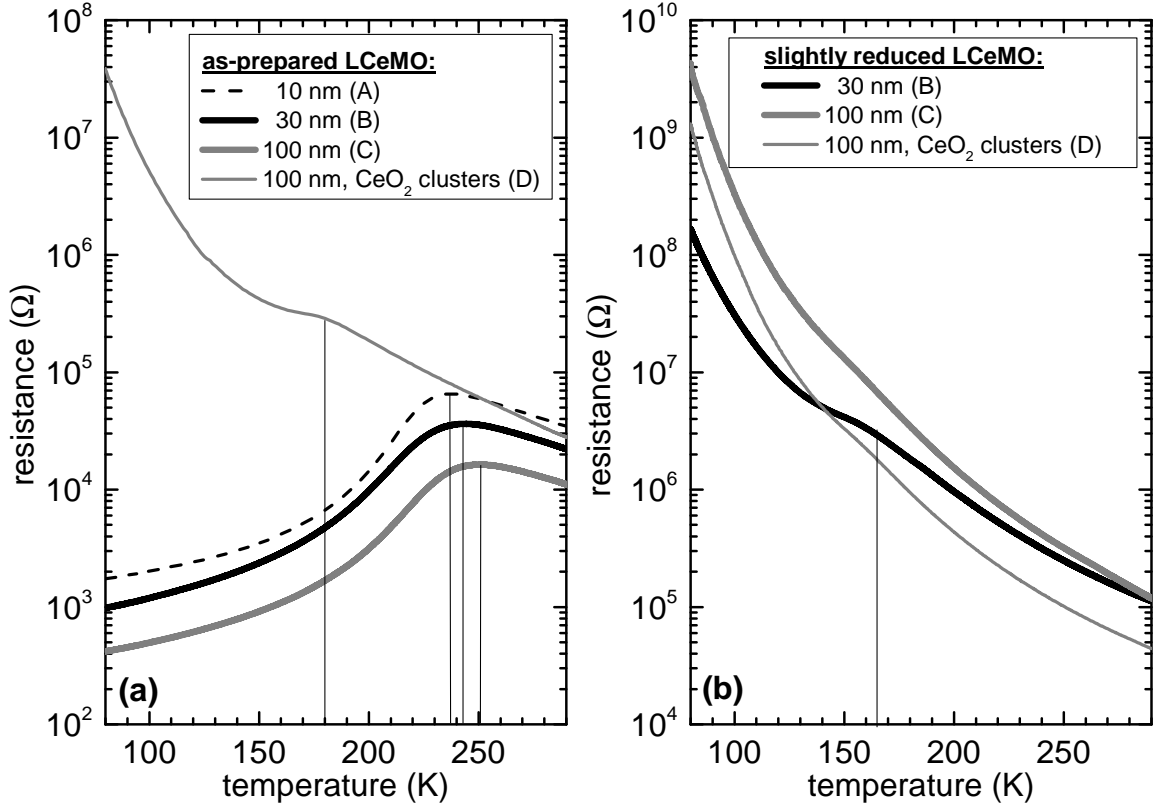


Figure 1. Resistance-vs.-temperature characteristics of the *as-prepared* LCeMO films (a), and the *slightly reduced* films (b). The vertical lines indicate the positions of the MITs, T_{MIT} , or the beginning of a plateau, T_{pl} , respectively.

3.3. Experimental findings for the manganites

Reviewing a number of currently available experimental studies of the temperature dependent transport in the insulating phase, the data was interpreted in terms of the APH model in refs. [18, 33, 34, 35, 36], while other authors [20, 21, 37, 38, 39] employed the Mott-VRH model or the ES-VRH model [20, 21, 25].

In general one can summarize that (i) for temperatures above 300 K the transport is determined by the carrier-lattice interaction, i.e., the thermally activated diffusion of small polarons being described by the APH model, while (ii) for lower temperatures carrier localization by disorder leads to hopping transport, which is described by the several variable-range hopping models.

4. Results

First, the resistance-vs.-temperature curves of the *as-prepared* films were recorded, as shown in figure 1(a). The samples A, B, and C show metal-insulator transitions (MITs) at 237 K, 243 K, and 251 K, respectively. The MIT temperatures (T_{MIT}) were extracted by smoothing and differentiating the R - T curves, looking for the points where the first derivatives of the respective R - T curve become zero. The values obtained are typical for LCeMO films with a hole doping by oxygen excess. The variation of the transition temperature with the film thickness is a well-known phenomenon and can be attributed to stronger relaxation of substrate-induced strain with growing film thickness.

Solely sample D does not exhibit an MIT, but a weak plateau at 180 K, which is commonly interpreted as a transition between a paramagnetic-insulating to a ferromagnetic-insulating phase and points towards an insufficient doping [40]. Obviously, the low oxygen partial pressure during the deposition of film D is the origin for the deviating R - T characteristics. As proven previously on an equivalent film [16], the MIT can be recovered by appropriate annealing under oxygen atmosphere.

The R - T curves in the insulating range between 300 K and 270 K can be reproduced by both the adiabatic polaron hopping (APH) and the variable-range hopping (VRH) model. A regression analysis assuming the APH model reveals polaron hopping energies of 115 mV for samples A, B, C, and 144 mV for sample D. According to the empirical relation, originally derived for $\text{La}_{0.7}\text{Ca}_{0.3}\text{MnO}_{3-\delta}$ [36]:

$$E_h = c(\text{Mn}^{3+}) \cdot 627 \text{ meV} - 377 \text{ meV} \quad , \quad (12)$$

§ The R - T curve of sample A is shown for the *as-prepared* case only to make the link to our previous investigations [14, 8], where this 10-nm film was in the focus.

Table 1. *As-prepared* and *slightly reduced* LCeMO films: Overview of the characteristic temperatures (either the temperature of the metal-insulator transition T_{MIT} or the plateau temperature T_{pl}), the polaron hopping energies E_h extracted from fitting with the APH model, and the corresponding Mn valences V_{Mn} according to eq. (12). For the slightly reduced films the Mn valences from our former XPS analysis [17] are given in brackets for comparison.

sample	thickness (nm)	CeO ₂ clusters	as-prepared state			slightly reduced state		
			T_{MIT}, T_{pl} (K)	E_h (meV)	V_{Mn}	T_{pl} (K)	E_h (meV)	$V_{Mn}(V_{Mn}^{XPS})$
B	30	nanoscopic	243 (MIT)	115	3.22	165	140	3.18 (3.19)
C	100	nanoscopic	251 (MIT)	115	3.22	–	165	3.14 (3.10)
D	100	microscopic	180 (pl.)	144	3.17	–	144	3.17 (3.31)

Table 2. *Highly reduced* LCeMO films: Overview of the fitting parameters derived from the APH model (columns 2–4) in the higher temperature range and from the respective (most suitable) VRH model in the lower temperature range (columns 5–10).

sample	adiabatic polaron hopping			variable-range hopping				
	range (K)	E_h (meV)	$V_{Mn}(V_{Mn}^{XPS})$	type	range (K)	T_{ES}, T_M (K)	a (nm)	Δ_C (eV)
B	300..210	281	– (2.81)	ES	below 210	1.06×10^5	0.3-0.6	0.41
C	300..210	228	2.96 (2.81)	ES	below 210	1.22×10^5	0.3-0.5	0.44
D (1 V)	300..260	52	2.68 (2.83)	Mott	260...80	6.61×10^8	0.09	–
D (5 V)	300..280	62	2.70 (2.83)	Mott	260...190	3.54×10^8	0.11	–

between the Mn^{3+} concentration $c(\text{Mn}^{3+})$ and the activation energy E_h for the APH process, we obtain a Mn^{3+} concentration of 78% for samples A, B, C. Since the *as-prepared* films had been shown to suffer from overoxygenation and concomitant hole doping [14, 16], it is reasonable to assume that the residual 22% of Mn ions have a valence of 4+. The corresponding average Mn valence is 3.22, being dramatically larger than the nominal Mn valence of 2.7, but being in good accordance with former results obtained on 10-nm thick as-prepared LCeMO films [14]. For sample D we obtain 83% Mn^{3+} and – due to the lower oxygen partial pressure during the film deposition – a smaller Mn valence of 3.17, which is still far above the nominal value.

The resistances of the *slightly reduced* films are decisively higher than in the as-prepared case [figure 1(b)]. Moreover, there are no clear MITs visible any longer, but a small plateau beginning at 165 K for sample B, while for C and D plateaus are hardly visible. Between 300 K and the plateau temperature the APH model gives hopping energies of 140 meV and 165 meV for B and C, respectively, which are higher than in the as-prepared cases and correspond to Mn valences of 3.18 (sample B) and 3.14 (sample C). These values are in good agreement with those derived from previous XPS results [17]. For sample D the same hopping energy as in the as-prepared case (144 meV) is extracted from the APH model, while the Mn valence from the present transport data (3.17) is lower than the value from XPS (3.31). One may speculate that the surface sensitivity of the XPS analysis combined with the higher disorder of sample D and the possible inhomogeneous oxygen diffusion during the oxygen-reducing annealing process are the origin for this discrepancy.

For clarity, all numeric results for the as-prepared and slightly reduced films are summarized in table 1.

As expected, the resistances of the *highly reduced* LCeMO films tend to be higher than in the slightly-reduced samples, see figures 2(a),(b). As an exception, the resistance of sample D at 1 V is higher in the slightly-reduced case between 275 K and 200 K, but within the same order of magnitude. At a measuring voltage of 1 V, all samples exhibit an insulating behavior in the whole investigated temperature range and no sign of a MIT.

Interestingly – and indeed electroresistive effects in LCeMO were reported in the past [41] – the resistance of film D strongly depends on the measuring voltage. As visible in figure 2(b), in the whole temperature range investigated here, the resistance at 5 V is clearly lower than at 1 V. Furthermore, at 5 V, an MIT appears at 135 K. Being beyond the scope of the present work, the clarification of the origin of this electrical-field induced MIT (intrinsic to the film or substrate-related) by comparative magnetoresistance investigations is currently in progress [42]. Note that the electroresistive effect turned out to be non-persistent and was observed solely in sample D.

Let us now, as in the cases of the as-prepared and the slightly-reduced films, continue with a detailed analysis of the resistances by curve fitting. For samples B and C, the R - T curves can be modeled by the APH model in the range between 300 K and 210 K. From this model we obtain polaron hopping energies of 281 meV (B) and 228 meV (C).

According to eq. (12) these hopping energies would be equivalent to a Mn^{3+} concentration of 96% for C, which is clearly different from the 81% from the former XPS investigation [17], while for B we get an unphysically high Mn^{3+} concentration of 105%, which causes some doubts on the validity of eq. (12), at least for the case of the highly reduced LCeMO films. Concerning the discrepancy of the XPS- and the transport related Mn^{3+} concentrations of sample C one could argue that there is a gradient of the Mn^{3+} concentration from the film surface towards deeper regions of the film and that XPS as a surface-sensitive method naturally detects only the value correct for the first few nanometers beneath

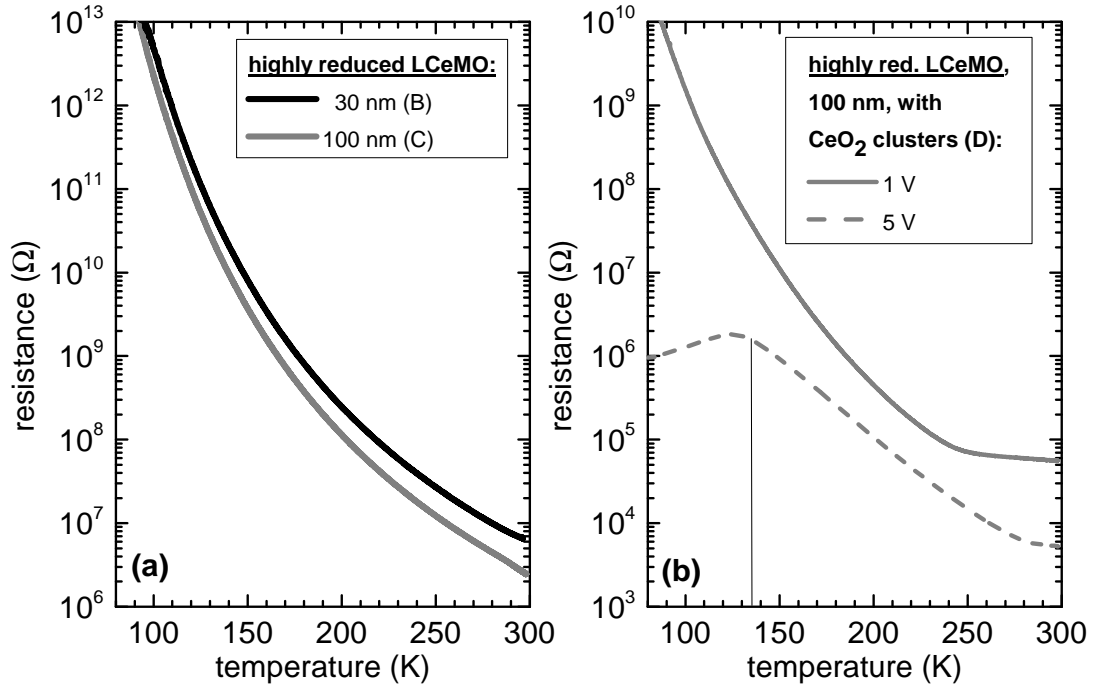


Figure 2. Resistance-vs.-temperature characteristics of the *highly reduced* LCeMO films: (a) Samples B and C; (b) sample D at two different measuring voltages (1 V, 5 V), showing an unexpected, pronounced electroresistive effect.

the surface. In other words, the films are stronger oxygen-deficient at the surface, which is indeed in agreement with the former x-ray absorption (XAS) results of comparable LCeMO films [16]. Furthermore, equation (12) is only valid when we assume the equivalence of Mn^{2+} and Mn^{4+} with respect to the double exchange mechanism, as proposed in the theoretical work by Schlottmann [12], which might also be questionable due to the high ionic radius of Mn^{2+} and the subsequent dramatic decrease of the Mn-O-Mn bond angle. Indeed such a electron-hole asymmetry regarding the double exchange in LCeMO was proposed by Middey et al. [15]. From these considerations, we have to state that both, the derivation of the Mn^{3+} concentration from the polaron hopping energy as well as from the XPS data, have to be understood as estimates.

The *comparative* analysis of the R - T data within the temperature range between 300 K and 90 K, testing the APH and the VRH models, is depicted in figure 3 (exemplified for the 100-nm samples C and D).

For *sample C*, as shown in figure 3(a), from 210 K towards lower temperatures the resistance increase with decreasing temperature is slower than expected from the APH model. The Mott-VRH model according to eq. (3) is not appropriate as well, since plotting of $\ln(R/T^{1/4})$ as a function of $T^{-1/4}$ does not result in a linear dependence. However, the modified Efros-Shklovskii VRH model [eqs. (10), (11)] reproduces the measured data in the whole considered temperature range very well. Accordingly, plotting $\ln(R/T^{9/2})$ versus $T^{-1/2}$ indeed results in a linear dependence. The fitting procedure yields a temperature independent $T_0 = 1.95 \times 10^5$ K. According to equation eq. (11) this means that the polaronic gap Δ_{pg} is proportional to $T^{1/2}$ like reported in refs. [25, 31]. Since the APH model starts to deviate from the measured data at $T_V = 210$ K it is appropriate to estimate Δ_{pg} as [31]:

$$\Delta_{pg} \approx E_h \left(\frac{T}{T_V} \right)^{1/2}. \quad (13)$$

With equation (11) and E_h from table 2 this yields $T_{ES} = 1.22 \times 10^5$ K.

Similarly, the transport data for *sample B* was evaluated and we deduce $T_0 = 1.92 \times 10^5$ K and $T_{ES} = 1.06 \times 10^5$ K (see also table 2). We stress that the Efros-Shklovskii VRH model is only valid for hopping energies $E_{ES}(T)$ [cf. eq. (8)] below the Coulomb gap Δ_C [eq. (9)]. Since even at 300 K no significant deviations between experimental and theoretical data occur, the Coulomb gap can be estimated as $\Delta_C \approx E_{ES}^{300\text{K}} = k_B \sqrt{T_{ES} \cdot 300\text{K}}$, resulting in values of 0.41 eV and 0.44 eV for samples B and C, respectively, which is in good agreement with the values for $\text{La}_{0.8}\text{Ca}_{0.2}\text{MnO}_3$ reported in ref. [32]. For an estimate of the electron localization length according to eq. (7) we need the permittivity, which we assume to be in the range of $\epsilon_r = 10 \dots 20$ according to literature values [43] for $\text{La}_{1-x}\text{Ca}_x\text{MnO}_3$. For samples B and C, we can now calculate localization lengths between 0.3 nm and 0.6 nm. Thus, the electrons are delocalized over several unit cells, as expected for magnetic polarons [19, 20].

For *sample D*, the resistance as a function of the temperature at a measuring voltage of 1 V is depicted in fig. 3(b). Between 300 K and 260 K the data is rebuilt by the APH model with a hopping energy of 52 meV. For a measuring voltage of 5 V, the same fitting procedure between 300 K and 280 K gives a slightly larger hopping energy of 62 meV. According to eq. (12) we obtain Mn^{3+} concentrations of 68% for $U = 1$ V and 70% for $U = 5$ V. Assuming a true electron doping,

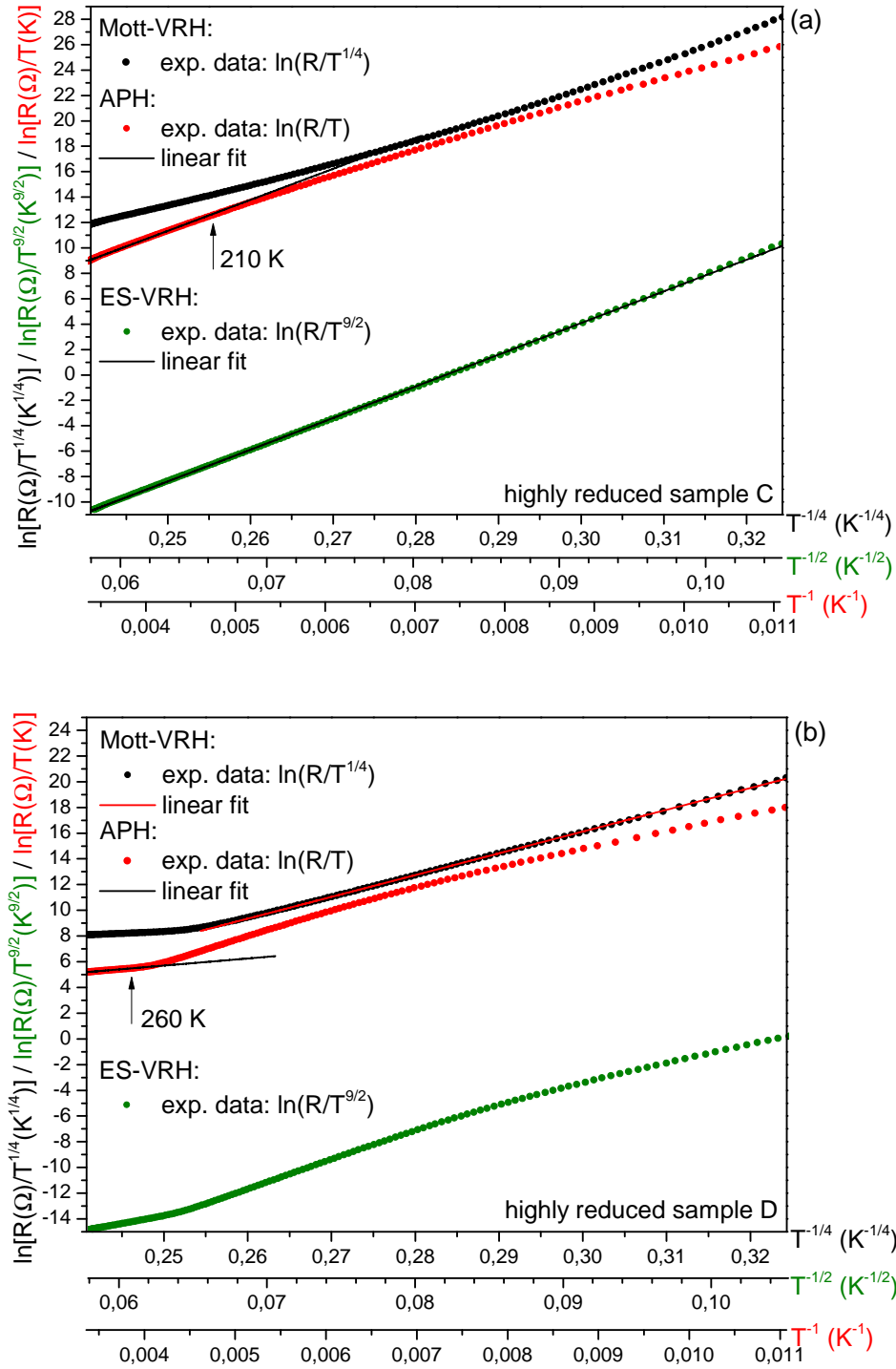


Figure 3. Highly reduced LCeMO films: Plots of the logarithms $\ln(R/T)$, $\ln(R/T^{1/4})$, and $\ln(R/T^{9/2})$ against T^{-1} , $T^{-1/4}$, and $T^{-1/2}$, respectively, for T between 300 K and 90 K in order to check the validity of either the APH, the Mott-VRH, or the modified ES-VRH model – exemplarily shown for samples C (a) and D (b); the data shown here was recorded at 1 V for both samples. The vertical arrows indicate the temperature below which one of the VRH models had to be used. For the exact fitting results refer to table 2.

i.e. a mixed $\text{Mn}^{2+/3+}$ valence, this would result in Mn valences of 2.68 or 2.70, which is – in contrast to the cases of samples B and C – lower than the XPS-derived value [17] of 2.83. A possible explanation might be that the high defect density in sample D supports a more uniform oxygen diffusion during the annealing process and not a reduction limited to the surface as for B and C.

For temperatures lower than 260 K the APH model fails to fit the experimental data, while, as shown in fig. 3(b), the Mott-VRH model eq. (3) reproduces the data acquired at 1 V measuring voltage very well down to 90 K, giving a VRH temperature of $T_M = 6.61 \times 10^8$ K. For the data measured at 5 V the fitting procedure results in $T_M = 3.54 \times 10^8$ K, in the temperature range between 280 K and 190 K. According to eq. (5) the average hopping energies read as 0.9 eV at 260 K and 0.37 eV at 90 K, which is decisively higher than the values for samples B and C, and must be explained with the stronger disorder in sample D (existence of microscopic CeO_2 clusters). Assuming a Coulomb gap of around 0.4 eV for sample D, too, it becomes clear why the ES-VRH model cannot reproduce the data appropriately: for that, the Coulomb gap would have to be larger than the hopping energy. The question why the activation energy jumps at 260 K, where we have changed the model for fitting the experimental data, from 52 meV (APH) to 900 meV (VRH) remains unsolved. One may speculate that the APH model is per se unsuitable for such a strongly disordered manganite film.

Finally, an estimate of the carrier localization length is made for sample D, too. For applying eq. (4) the density of states at the Fermi energy is needed, which we extract from the formula given by Viret et al. [20] as follows:

$$N(E_F) = \frac{0.5x(1-x)}{V_{uc}U_H}, \quad (14)$$

with $(1-x)$ being the concentration of the Mn^{3+} ions, V_{uc} being the unit cell volume, and $U_H = 2$ eV the Hundt coupling energy. With $x = 0.17$ from our former XPS measurements [17] and a lattice constant of $c = 0.3894$ nm, a density of states of $N(E_F) = 5.95 \times 10^{26} \text{ m}^{-3} \text{ eV}^{-1}$ is calculated, which results in localization lengths of 0.09 nm and 0.11 nm for measuring voltages of 1 V and 5 V, respectively. At 260 K, the average hopping distance according to eq. (5) is 3.6 nm for both voltages, i.e., the electrons are mainly localized at the Mn ions and have to hop over approximately 10 lattice constants to find a place with suitable energy. For an overview of the numerical data extracted from fitting the transport data of the highly reduced films refer to table 2.

5. Summary

The resistance-vs.-temperature characteristics of $\text{La}_{0.7}\text{Ce}_{0.3}\text{MnO}_3$ films of different thickness, oxygen reduction, and CeO_2 phase segregation have been recorded in the range between 300 K and 90 K. While the film thickness regarded here (up to 100 nm) has only a slight influence on the electrical transport, successive oxygen reduction leads – as observed in other manganite compounds as well – to a dramatic increase of the resistance and the loss of the manganite-typical metal-insulator transition. As expected from a number of previous results, only the highly reduced LCeMO films exhibited a Mn valence below 3+ and thus an effective electron doping. Depending on the degrees of oxygen deficiency and CeO_2 segregation as well as on the temperature range, very individual states of disorder are prepared in the respective LCeMO films, which result in different transport mechanisms with widely scattered values for the hopping energies and the carrier localization lengths.

Acknowledgement

This work was kindly supported by the German Science Foundation (DFG, grant no. BE 3804/2-1).

References

- [1] J. M. D. Coey, M. Viret, and S. von Molnar. Mixed-valence manganites. *Adv. Phys.*, 48(2):167–293, 1999. doi:10.1080/000187399243455.
- [2] A.-M. Haghiri-Gosnet and J.-P. Renard. CMR manganites: physics, thin films and devices. *J. Phys. D: Appl. Phys.*, 36(8):R127–R150, 2003. doi:10.1088/0022-3727/36/8/201.
- [3] J. Volger. Further experimental investigations on some ferromagnetic oxidic compounds of manganese with perovskite structure. *Physica*, 20:49–66, 1954. doi:10.1016/S0031-8914(54)80015-2.
- [4] P. W. Anderson and H. Hasegawa. Considerations on double exchange. *Phys. Rev.*, 100:675–681, 1955. doi:10.1103/PhysRev.100.675.
- [5] A. J. Millis, R. Mueller, and B. I. Shraiman. Fermi-liquid-to-polaron crossover. II. Double exchange and the physics of colossal magnetoresistance. *Phys. Rev. B*, 54(8):5405–5417, 1996. doi:10.1103/PhysRevB.54.5405.
- [6] R. von Helmholt, R. Wecker, B. Holzapfel, L. Schultz, and K. Samwer. Giant negative magnetoresistance in perovskitelike $\text{La}_{2/3}\text{Ca}_{1/3}\text{MnO}_3$ ferromagnetic films. *Phys. Rev. Lett.*, 71:2331–2334, 1993. doi:10.1103/PhysRevLett.71.2331.
- [7] E. Dagotto. Colossal magnetoresistant materials: The key role of phase separation. *Phys. Rep.*, 344:1–153, 2001. doi:10.1016/S0370-1573(00)00121-6.
- [8] E. Beyreuther, A. Thiessen, S. Grafström, L. M. Eng, M. C. Dekker, and K. Dörr. Large photoconductivity and light-induced recovery of the insulator-metal transition in ultrathin $\text{La}_{0.7}\text{Ce}_{0.3}\text{MnO}_{3-\delta}$ films. *Phys. Rev. B*, 80:075106, 2009. doi:10.1103/PhysRevB.80.075106.
- [9] H. Tanaka, J. Zhang, and T. Kawai. Giant Electric Field Modulation of Double Exchange Ferromagnetism at Room Temperature in the Perovskite Manganite/Titanate p-n Junction. *Phys. Rev. Lett.*, 88(2):027204, 2001. doi:10.1103/PhysRevLett.88.027204.
- [10] C. Mitra, P. Raychaudhuri, G. Köbernik, K. Dörr, K.-H. Müller, L. Schultz, and R. Pinto. p-n diode with hole- and electron-doped lanthanum manganites. *Appl. Phys. Lett.*, 79(15):2408–2410, 2001. doi:10.1063/1.1409592.

- [11] C. Mitra, P. Raychaudhuri, K. Dörr, K.-H. Müller, L. Schultz, P. M. Oppeneer, and S. Wirth. Observation of Minority Spin Character of the New Electron Doped Manganite $\text{La}_{0.7}\text{Ce}_{0.3}\text{MnO}_3$ from Tunneling Magnetoresistance. *Phys. Rev. Lett.*, 90(1):017202, 2003. doi:10.1103/PhysRevLett.90.017202.
- [12] P. Schlottmann. Phase diagram and spin-canting effects in electron-doped LaMnO_3 . *Phys. Rev. B*, 77:104446, 2008. doi:10.1103/PhysRevB.77.104446.
- [13] P. Raychaudhuri, C. Mitra, P. D. A. Mann, and S. Wirth. Phase diagram and Hall effect of the electron doped manganite $\text{La}_{1-x}\text{Ce}_x\text{MnO}_3$. *J. Appl. Phys.*, 93(10):8328–8330, 2003. doi:10.1063/1.1556976.
- [14] E. Beyreuther, S. Grafström, L. M. Eng, C. Thiele, and K. Dörr. XPS investigation of Mn valence in lanthanum manganite thin films under variation of oxygen content. *Phys. Rev. B*, 73:155425, 2006. doi:10.1103/PhysRevB.73.155425.
- [15] S. Middey, M. Kareev, D. Meyers, X. Liu, Y. Cao, S. Tripathi, D. Yazici, M. B. Maple, P. J. Ryan, J. W. Freeland, and J. Chakhalian. Epitaxial stabilization of ultra thin films of electron doped manganites. *Appl. Phys. Lett.*, 104:202409, 2014. doi:10.1063/1.4879456.
- [16] R. Werner, C. Raisch, V. Leca, V. Ion, S. Bals, G. Van Tendeloo, T. Chassé, R. Kleiner, and D. Koelle. Transport, Magnetic, and Structural Properties of $\text{La}_{0.7}\text{Ce}_{0.3}\text{MnO}_3$ Thin Films: Evidence for Hole-Doping. *Phys. Rev. B*, 79:054416, 2009. doi:10.1103/PhysRevB.79.054416.
- [17] A. Thiessen, E. Beyreuther, S. Grafström, K. Dörr, R. Werner, R. Kleiner, D. Koelle, and L. M. Eng. The $\text{Mn}^{2+}/\text{Mn}^{3+}$ state of $\text{La}_{0.7}\text{Ce}_{0.3}\text{MnO}_3$ by oxygen reduction and photodoping. *J. Phys.: Condens. Matter*, 26:045502, 2014. doi:10.1088/0953-8984/26/4/045502.
- [18] D.C. Worledge, L. Mieville, and T. H. Geballe. On-site Coulomb repulsion in the small polaron system $\text{La}_{1-x}\text{Ca}_x\text{MnO}_3$. *Phys. Rev. B*, 57:15267, 1998. doi:10.1103/PhysRevB.57.15267.
- [19] J. M. D. Coey, M. Viret, L. Ranno, and K. Ounadjela. Electron Localization in Mixed-Valence Manganites. *Phys. Rev. Lett.*, 75:3910–3913, 1995. doi:10.1103/PhysRevLett.75.3910.
- [20] M. Viret, L. Ranno, and J. M. D. Coey. Magnetic localization in mixed-valence manganites. *Phys. Rev. B*, 55(13):8067–8070, 1997. doi:10.1103/PhysRevB.55.8067.
- [21] P. Wagner, I. Gordon, L. Trappeniers, J. Vanacken, F. Herlach, V. V. Moshchalkov, and Y. Bruynseraede. Spin Dependent Hopping and Colossal Negative Magnetoresistance in Epitaxial $\text{Nd}_{0.52}\text{Sr}_{0.48}\text{MnO}_3$ Films in Fields up to 50 T. *Phys. Rev. Lett.*, 81:3980, 1998. doi:10.1103/PhysRevLett.81.3980.
- [22] M. B. Salomon and M. Jaime. The physics of manganites: Structure and transport. *Rev. Mod. Phys.*, 73:583–628, 2001. doi:10.1103/RevModPhys.73.583.
- [23] D. M. Edwards. Ferromagnetism and electron-phonon coupling in the manganites. *Adv. Phys.*, 51(5):1259–1318, 2002. doi:10.1080/00018730210140805.
- [24] Y. Sun, X. Xu, and Y. Zhang. Variable-range hopping of small polarons in mixed-valence manganites. *J. Phys.: Condens. Matter*, 12:10475–10480, 2000. doi:10.1088/0953-8984/12/50/309.
- [25] R. Laiho, K. G. Lisunov, E. Lähderanta, P. A. Petrenko, J. Salminen, M. A. Shakhov, M. O. Safontchik, V. S. Stamov, M. V. Shubnikov, and V. S. Zakhvalinskii. Variable-range hopping conductivity in $\text{La}_{1-x}\text{Ca}_x\text{Mn}_{1-y}\text{Fe}_y\text{O}_3$: evidence of a complex gap in density of states near the Fermi level. *J. Phys.: Condens. Matter*, 14:8043–8055, 2002. doi:10.1088/0953-8984/14/34/323.
- [26] H. Fröhlich, H. Pelzer, and S. Zienau. Properties of slow electrons in polar materials. *Phil. Mag.*, 41:221–241, 1950. doi:10.1080/14786445008521794.
- [27] N. Tsuda, K. Nasu, A. Fujimori, and K. Siratori. *Electronic Conduction in Oxides*. Springer, Berlin – Heidelberg – New York, 2000.
- [28] N. F. Mott and E. A. Davis. *Electronic Processes in Non-Crystalline Materials*. Oxford University Press, Oxford-New York, 2012.
- [29] C. H. Seager and G. E. Pike. Percolation and conductivity: A computer study. II. *Phys. Rev. B*, 10:1435–1446, 1974. doi:10.1103/PhysRevB.10.1435.
- [30] A. L. Efros and B. I. Shklovskii. Coulomb gap and low temperature conductivity of disordered systems. *J. Phys. C: Solid State Phys.*, 8:L49–L51, 1975. doi:10.1088/0022-3719/8/4/003.
- [31] R. Laiho, K. G. Lisunov, E. Lähderanta, M. A. Shalkov, V. N. Stamov, V. S. Zakhvalinskii, V. L. Kozhevnikov, I. A. Leonidov, E. B. Mitberg, and M. V. Patrakeev. Mechanisms of hopping conductivity in weakly doped $\text{La}_{1-x}\text{Ba}_x\text{MnO}_3$. *J. Phys.: Condens. Matter*, 17:3429, 2005. doi:10.1088/0953-8984/17/21/033.
- [32] A. Biswas, S. Elizabeth, A. K. Raychaudhuri, and H. L. Bhat. Density of states of hole-doped manganites: A scanning-tunneling-microscopy/spectroscopy study. *Phys. Rev. B*, 59(8):5368–5376, 1999. doi:10.1103/PhysRevB.59.5368.
- [33] M. Jaime, M. B. Salamon, M. Rubinstein, R. E. Treece, J. S. Horwitz, and D. B. Chrisey. High-temperature thermopower in $\text{La}_{2/3}\text{Ca}_{1/3}\text{MnO}_3$ films: Evidence for polaronic transport. *Phys. Rev. B*, 54:11914–11917, 1996. doi:10.1103/PhysRevB.54.11914.
- [34] G. J. Snyder, R. Hiskes, S. DiCarolis, M. R. Beasley, and T. H. Geballe. Intrinsic electrical transport and magnetic properties of $\text{La}_{0.67}\text{Ca}_{0.33}\text{MnO}_3$ and $\text{La}_{0.67}\text{Sr}_{0.33}\text{MnO}_3$ MOCVD thin films and bulk material. *Phys. Rev. B*, 53(21):14434–14444, 1996. doi:10.1103/PhysRevB.53.14434.
- [35] G. Jakob, W. Westerburg, F. Martin, and H. Adrian. Small-polaron transport in $\text{La}_{0.67}\text{Ca}_{0.33}\text{MnO}_3$ thin films. *Phys. Rev. B*, 58:14966–14970, 1998. doi:10.1103/PhysRevB.58.14966.
- [36] J. M. De Teresa, K. Dörr, K. H. Müller, L. Schultz, and R. I. Chakalova. Strong influence of the Mn^{3+} content on the binding energy of the lattice polarons in manganese perovskites. *Phys. Rev. B*, 58:R5928, 1998. doi:10.1103/PhysRevB.58.R5928.
- [37] J. M. De Teresa, M. R. Ibarra, J. Blasco, J. Garcia, C. Marquina, P. A. Algarabel, Z. Arnold, K. Kamenev, C. Ritter, and R. von Helmolt. Spontaneous behavior and magnetic field and pressure effects on $\text{La}_{2/3}\text{Ca}_{1/3}\text{MnO}_3$ perovskite. *Phys. Rev. B*, 54:1187, 1996. doi:10.1103/PhysRevB.54.1187.
- [38] M. Jaime, M. B. Salamon, K. Pettit, M. Rubinstein, R. E. Treece, J. S. Horwitz, and D. B. Chrisey. Magnetothermopower in $\text{La}_{0.67}\text{Ca}_{0.33}\text{MnO}_3$ thin films. *Appl. Phys. Lett.*, 68:1576–1578, 1996. doi:10.1063/1.116686.
- [39] J. M. De Teresa, M. R. Ibarra, P. A. Algarabel, C. Ritter, C. Marquina, J. Blasco, J. Garcia, A. del Moral, and Z. Arnold. Evidence for magnetic polarons in the magnetoresistive perovskites. *Nature*, 386:256, 1997. doi:10.1038/386256a0.
- [40] A. Seeger, P. Lunkenheimer, J. Hemberger, A. A. Mukhin, V. Y. Ivanov, A. M. Balbashov, and A. Loidl. Charge carrier localization in $\text{La}_{1-x}\text{Sr}_x\text{MnO}_3$ investigated by ac conductivity measurements. *J. Phys.: Condens. Matter*, 11:3273, 1999. doi:10.1088/0953-8984/11/16/009.
- [41] K. Bajaj, J. Jesudasan, V. Bagwe, D. C. Kothari, and P. Raychaudhuri. Electroresistive effects in electron doped manganite $\text{La}_{0.7}\text{Ce}_{0.3}\text{MnO}_3$ thin films. *J. Phys.: Condens. Matter*, 19:046208, 2007. doi:10.1088/0953-8984/19/4/046208.
- [42] A. Thiessen, E. Beyreuther, R. Werner, R. Kleiner, D. Koelle, and L. M. Eng. Conductivity and magnetoresistance of $\text{La}_{0.7}\text{Ce}_{0.3}\text{MnO}_3$ films under photoexcitation. 2014. URL: <http://arxiv.org/abs/1408.4909>.
- [43] K. P. Neupane, J. L. Cohn, H. Terashita, and J. J. Neumeier. Doping dependence of polaron hopping energies in $\text{La}_{1-x}\text{Ca}_x\text{MnO}_3$ ($0 \leq x \leq 0.15$). *Phys. Rev. B*, 74:144428, 2006. doi:10.1103/PhysRevB.74.144428.